COBEM 2021 26th International Congress of Mechanical Engineering
November 22-26, 2021, Virtual Congress, Brazil
ABCM Associação Brasileira de Engenharia e Ciências Mecânicas

COB-2021-1378
MODELING AND SIMULATION OF AQUEOUS HUMOUR FLOW IN THE HUMAN EYE

Caio Vinícius Schurgelies de Sá
André von Borries Lopes
Departamento de Engenharia Mecânica, Universidade de Brasília. Campus Universitário Darcy Ribeiro, DF 70910-900, Brazil.
caioschurgelies@gmail.com
andre.lopes@unb.br

Abstract. *We revisit simple physical models for the fluid flow of aqueous humour in the anterior chamber of the human eye, comparing analytical solutions previously obtained in literature with numerical simulations. A brief introduction of basic eye physiology is presented. Buoyancy driven forces forces are present in the studied flow, due to a small thermal gradient, and hence we use the Boussinesq approximation to present the governing equations of mass, linear momentum and energy, with proper boundary conditions. We employ the so-called lubrication theory, due to the shallow geometry of the anterior chamber, to simplify the governing equations and solve them analytically. We then implement a numerical simulation using the SU2 finite volume code, assuming laminar steady flow. The numerical solution is compared with the analytical one, showing that the two approaches are in good agreement considering the general flow behaviour. The analytical solution, however, does not capture all its features, what was attributed mainly to over simplifications in the energy equation. We also conclude that the buoyancy driven flow is the dominant mechanism inside the anterior chamber.*

Keywords: *lubrication theory, Boussinesq's approximation, anterior chamber, SU2*

1. INTRODUCTION

1.1 Fluid mechanics in biomedical sciences

High fidelity numerical simulations are employed to a large range of technological applications, with costs and response time compatibles with industrial demand. In this context, computational fluid mechanics (CFD) has presented itself as a promising tool to the advance of biomedical sciences. Among the benefits are a deeper understanding of physiological functions, the developing of clinical treatments and the design of biomedical devices, with examples like artificial valves in cardiovascular medicine and study of the effects of septum deviation in nasal flow.

Mathematical models and numerical analysis of the physiology of the human eye are also presenting promising results in recent years. Important flow occur in and around the eye, some of them related to thermal processes, like the aqueous humour flow in the anterior chamber, object of the present study. There is much progress to be made in ocular diseases treatment, and this justifies the interest in improving human eye models with fluid mechanics simulations input.

1.2 Anterior chamber and aqueous humour flow

The eye is arranged internally in some tissues and three chambers filled with fluids, namely anterior, posterior and vitreous. Anterior and posterior chambers are filled with a transparent liquid called aqueous humour, and vitreous chamber is filled with a jelly-like substance named vitreous humour.

The anterior chamber is bounded mainly by the corneal endothelium, the anterior surface of the iris and the pupil aperture. The cornea meets the iris at the chamber edge, forming the anterior chamber angle, where a draining apparatus is located (see Fig. 1). Aqueous humour is continuously produced by the ciliary body from blood plasma. After released, it flows along the posterior chamber, between the iris and the lens, entering the anterior chamber through the pupil aperture, where it flows until being drained at the anterior chamber angle. The main way out is through the trabecular meshwork, an intricate net of conjunctive tissue that carries the aqueous humour to Schlemm's channel, where it is collected and ultimately sent to episcleral veins, according to Fatt and Weissman (2013).

Aqueous humour in mainly constituted by water (98%). Other significant compounds, according to Goel *et al.* (2010), are organic and inorganic ions, carbohydrates, glutathione, urea, amino acids, proteins, oxygen and carbon dioxide.

Fluorescein, a dye usually employed as flow tracer, can be used to clinical observation of aqueous humour flow. After topical application at the cornea, diffusion to the anterior chamber occurs, where its concentration is measured over a few hours. Brubaker (1997) determined flows of $3,0 \pm 0,8\,\mu\mathrm{L/min}$ in the morning and $2,7 \pm 0,6\,\mu\mathrm{L/min}$ in the afternoon,

corresponding to a 1–2% renew in the chamber volume per minute. The notion that thermal processes also have an important role in aqueous humour flow is well established in ophthalmology, due to the thermal gradient in the anterior chamber. The iris is maintained basically at the core body temperature, $37°\mathrm{C}$, while the corneal endothelium experiences a temperature very close that of the eye surface. The latter can be measured using infrared thermography, with Ng and Ooi (2007) indicating an average of $34,5°\mathrm{C}$. This gradient, usually at the range of 1–$3°\mathrm{C}$, leads to convection of aqueous humour.

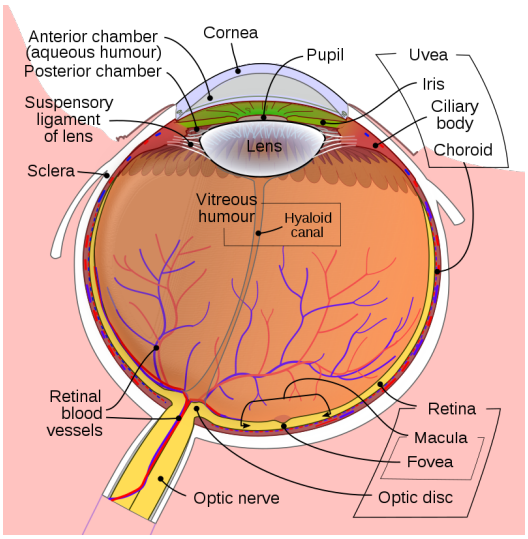

Figure 1. Eye's anatomy. By Rhcastilhos and Jmarchn, CC BY-SA 3.0, <https://creativecommons.org/licenses/by-sa/3.0>, via Wikimedia Commons.

A balance between production, circulation and drainage of aqueous humour is fundamental to preserve the functions of the healthy eye. Elevation in outflow resistance due to morphological modifications in the drainage apparatus increases intraocular pressure to abnormal levels, one of the major causes of glaucoma. Therefore, aqueous humour dynamics, especially related with drainage and obstruction processes, isn't entirely known, making it a bottleneck to more efficient glaucoma treatments, according to Tamm (2015).

Canning *et al.* (2002) proposed a mathematical and physical model to aqueous humour flow in the anterior chamber, based on Boussinesq approximation and lubrication theory. Considering only the inflow and outflow (isothermal problem) or, alternatively, only the convective flow (suppressing inflow and outflow), the model has an analytical solution, under certain simplifications.

A higher fidelity model for eye related flows, including both mechanisms cited previously, demands a numerical implementation of the incompressible Navier-Stokes equations, to a representative anterior chamber geometry. With this is mind, Kumar *et al.* (2006) included trabecular meshwork effects, while Karampatzakis and Samaras (2010) considered the thermal problem of the complete eyeball, although suppressing aqueous inflow and outflow. The present study starts from Canning *et al.* (2002) model to implement a more detailed simulations using finite volumes, with results comparison and discussion of physiological implications.

2. REDUCED MODEL

2.1 Geometrical modeling

A model of the anterior chamber (see Fig. 2) can be defined, in Cartesian coordinates (x, y, z), using the surfaces $z = f(x, y)$, representing the iris/pupil, and $z = h(x, y)$, representing the cornea. Canning *et al.* (2002) suggested the plane $z = 0$ for the iris/pupil and the expression

$$h(x, y) = h_0 \left(1 - \frac{x^2 + y^2}{a^2}\right) \tag{1}$$

to describe the cornea mathematically, where a and h_0 are, respectively, the anterior chamber radius and height. T_1 expresses the temperatures of the iris and T_0 the temperature of the cornea.

2.2 Governing equations

As discussed previously, the temperature gradient $T_1 - T_0 \sim 3°\mathrm{C}$ characterizes a thermal flow in anterior chamber, suitable for Boussinesq approximation use. Accordingly to Pontes and Mangiavacchi (2016), in this classical approach,

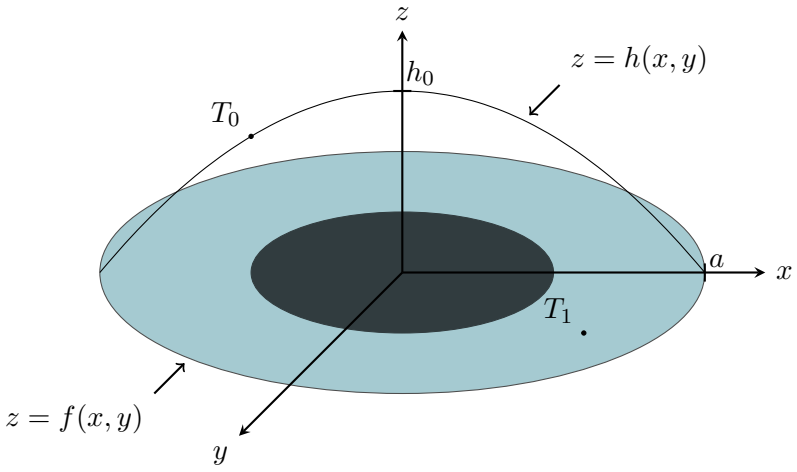

Figure 2. Geometrical model of the anterior chamber.

all fluid properties can be set as constant within small temperature variations, except in the buoyancy term of the Navier-Stokes equations. For that, the compressibility effect must be considered, leading to the following expression for density

$$\rho = \rho_0 \left[1 - \alpha(T - T_0)\right], \tag{2}$$

where T_0 and $\rho_0 = \rho_0(T_0)$ are reference values and α is the coefficient of linear thermal expansion of the fluid. Thus the governing equations are the Navier-Stokes equations, including mass, linear momentum and energy balance, in the Boussinesq approximation:

$$\boldsymbol{\nabla} \cdot \boldsymbol{u} = 0, \tag{3}$$

$$\rho_0(\partial_t \boldsymbol{u} + \boldsymbol{u} \cdot \boldsymbol{\nabla}\boldsymbol{u}) = -\boldsymbol{\nabla} p + \mu \nabla^2 \boldsymbol{u} + \rho_0[1 - \alpha(T - T_0)]\boldsymbol{g}, \tag{4}$$

$$\partial_t T + \boldsymbol{u} \cdot \boldsymbol{\nabla} T = \frac{k}{\rho_0 c_p} \nabla^2 T, \tag{5}$$

where $\boldsymbol{u}(x, y, z, t) = u\boldsymbol{i} + v\boldsymbol{j} + w\boldsymbol{k}$ is the velocity field, $p = p(x, y, z, t)$ is the pressure field, μ is the dynamic viscosity, $\boldsymbol{g}$ is the gravitation acceleration and t denotes time. Gravity acts along the positive direction of x axis when the patient is in standing position, and along the negative direction of z axis when he is lying down. In the temperature equation, k is the coefficient of thermal conductivity and c_p is the specific heat at constant pressure.

2.3 Scaling

Following Canning *et al.* (2002), the governing equations of motion are simplified by means of the lubrication approximation. The aspect ratio,

$$\epsilon = \frac{h_0}{L}, \tag{6}$$

where $L = 2a$, is used to introduce the dimensionless variables (denoted by a tilde): $x = L\widetilde{x}$, $y = L\widetilde{y}$, $z = \epsilon L\widetilde{z}$, $u = U\widetilde{u}$, $v = U\widetilde{v}$, $w = \epsilon U\widetilde{w}$, $t = L\widetilde{t}/U$, $T = (T_1 - T_0)\widetilde{T} + T_0$ and $p = \mu U L\widetilde{p}/h_0^2$. The characteristic speed U has an estimated order of magnitude of $10^{-4}\,\mathrm{m/s}$ (to be verified *a posteriori*). Table 1 presents the typical values used to calculate Reynolds, Froude and Péclet numbers, in addition to the aspect ratio, as follows:

$$\mathit{Re} = \frac{\rho_0 U L}{\mu} \sim 2, \quad \mathit{Fr} = \frac{U}{\sqrt{gL}} \sim 0,0003, \quad \mathit{Pe} = \frac{UL}{\alpha} \sim 9, \quad \epsilon \sim 0,2. \tag{7}$$

By considering the reduced Reynolds number $\epsilon^2 \mathit{Re}$ to be small, we have a viscous dominated flow (inertia effects are negligible), which leads to a significant simplification of the governing equations. The dimensionless energy equation

$$\frac{D\widetilde{T}}{D\widetilde{t}} = \frac{1}{\mathit{Pe}} \left(\frac{\partial^2 \widetilde{T}}{\partial \widetilde{x}^2} + \frac{\partial^2 \widetilde{T}}{\partial \widetilde{y}^2} + \frac{1}{\epsilon^2} \frac{\partial^2 \widetilde{T}}{\partial \widetilde{z}^2} \right), \tag{8}$$

however, requires a more careful analysis. The proposed scaling shows that the diffusive term with respect to x and y can be suppressed without controversy. Nevertheless, the $\partial^2 T/\partial z^2 = O(1/\mathit{Pe}\epsilon^2) \sim 2$ term, ruled by the reduced Péclet

Table 1. Geometric and physical parameters of the anterior chamber and aqueous humor (AH)

Symbol	Parameter	Typical value
a	Anterior chamber radius (m)[a]	$6,27 \times 10^{-3}$
h_0	Anterior chamber height (m)[a]	$2,99 \times 10^{-3}$
k	AH thermal conductivity (W/m/K)[b]	$0,578$
ρ_0	AH density ($\mathrm{kg/m^3}$)[c]	$994,1$
ν	AH cinematic viscosity ($\mathrm{m^2/s}$)[c]	$7,25 \times 10^{-7}$
α	AH linear expansion coefficient (/K)[c]	$3,4 \times 10^{-4}$
c_p	AH specific heat at constant pressure (J/kg/K)[c]	4178
g	Gravitational acceleration ($\mathrm{m/s^2}$)	$9,81$

[a] Goldsmith *et al.* (2005).
[b] Poppendiek *et al.* (1967).
[c] Batchelor (1967). Water properties at 35°C.

number, has the same order of magnitude of the convective term $\mathrm{D}T/\mathrm{D}t = O(1)$. If we choose to retain those two terms, we will be unable to find a closed expression for temperature, and an analytical solution of the governing system of equations would not be possible. Aiming an analytical solution, we follow Canning *et al.* (2002) and suppress the convective terms. Although with this methodology we can obtain average parameters in good agreement with those of clinical observations, this simplification certainly dissipates local mechanisms of the flow, which aren't captured. This simplification, together with others previously discussed, will be revisited after the numerical results. For now, under these assumptions, we obtain the following equations for a patient in standing position

$$\frac{\partial u}{\partial x} + \frac{\partial v}{\partial y} + \frac{\partial w}{\partial z} = 0, \tag{9}$$

$$-\frac{\partial p}{\partial x} + \mu\frac{\partial^2 u}{\partial z^2} + \rho_0 g[1 - \alpha(T_1 - T_0)T] = 0, \tag{10}$$

$$-\frac{\partial p}{\partial y} + \mu\frac{\partial^2 v}{\partial z^2} = 0, \tag{11}$$

along with $\partial p/\partial z = 0$ and $\partial^2 T/\partial z^2 = 0$. The boundary conditions are $u = v = 0$ at $z = 0$ (no-slip) and $u = v = w = 0$ at $z = h(x, y)$, the aqueous humour inflow/outflow condition $w = w_0(x, y)$ at $z = 0$ and a reference pressure p_a at $x = -a$.

The velocity components u and v are easily derived from integration of Eqs. (10) and (11), respectively, and w component is obtained by substituting into Eq. (9), all three as functions of $p(x, y)$. A closed form expression for the pressure expression is not possible in general if $w_0 = w_0(x, y)$, so we assume $w_0 = 0$, and then integrate Eq. (9), limiting the flow to thermal effects only.

Therefore, we obtain a linear expression for pressure and a two-dimensional velocity field (Fig. 3), with $v = 0$ and streamlines restricted to planes given by $y =$ constant:

$$p = p_a + (x + a)g\rho_0\left[1 - \frac{\alpha(T_1 - T_0)}{2}\right], \tag{12}$$

$$u = -\frac{(T_1 - T_0)\rho_0 g\alpha}{12\mu h} z(2z - h)(z - h), \tag{13}$$

$$w = -\frac{(T_1 - T_0)\rho_0 g\alpha}{24\mu h^2}\frac{\partial h}{\partial x} z^2(z^2 - h^2). \tag{14}$$

Using the analytical solution, some important parameters can be determined. For $y = 0$, we have

$$|u|_{\text{max}} \sim (T_1 - T_0)\, 3,3 \times 10^{-4}\,\mathrm{m/s} \tag{15}$$

and

$$|u|_{\text{avg}} \sim (T_1 - T_0)\, 1,0 \times 10^{-4}\,\mathrm{m/s}, \tag{16}$$

where the subscripts max and avg stand for maximum and average, respectively. These values are compatible with the estimates given in the scaling of the problem.

Shear stress τ at the iris can be calculated using the following expression:

$$\tau = \rho_0\nu \left.\frac{\partial u}{\partial z}\right|_{z=0} = -\frac{(T_1 - T_0)g\alpha\rho_0 h}{12}, \tag{17}$$

assuming a maximal $\tau_{\text{max}} = -(T_1 - T_0)\, 8,3 \times 10^{-4}\,\mathrm{kg/m/s^2}$, at the virtual center of the iris.

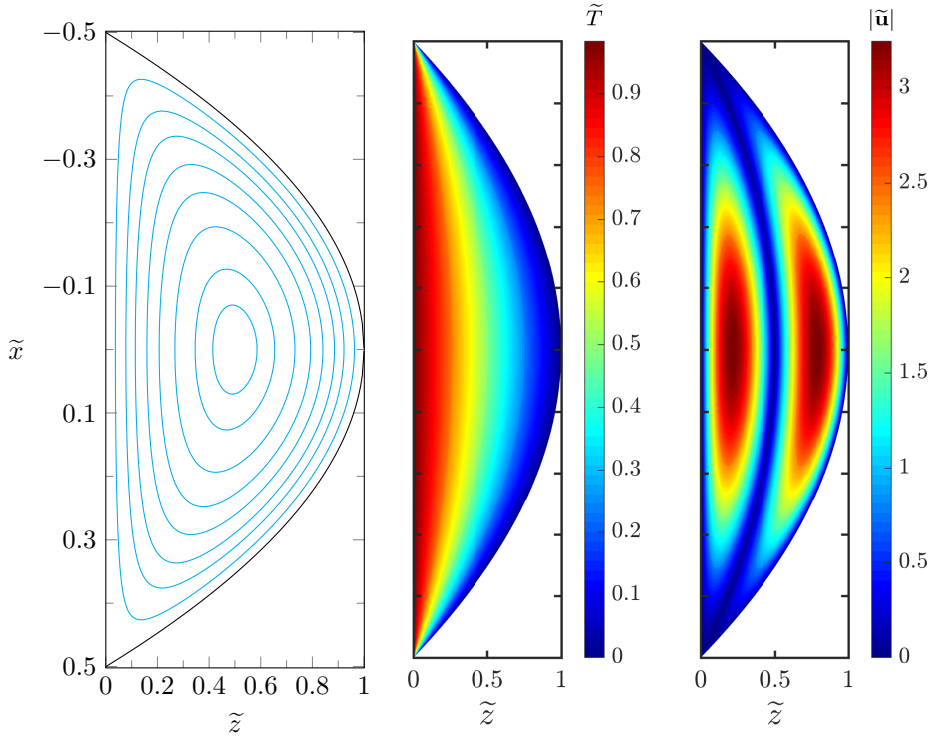

Figure 3. Streamlines of the analytical solution, non-dimensional temperature contours and non-dimension velocity contours at $\widetilde{y} = 0$. The patient is standing up, without flow through the pupil.

3. NUMERICAL SIMULATIONS

The numerical simulation was run using SU2 v7.0.5, an open source code based on C++ for partial differential equations, with support of a variety of fluid mechanics models. We employed the Navier-Stokes equations with Boussinesq model to density, using the steady version of Eqs. (3)—(5). The flow was solved considering laminar regime, with constant viscosity.

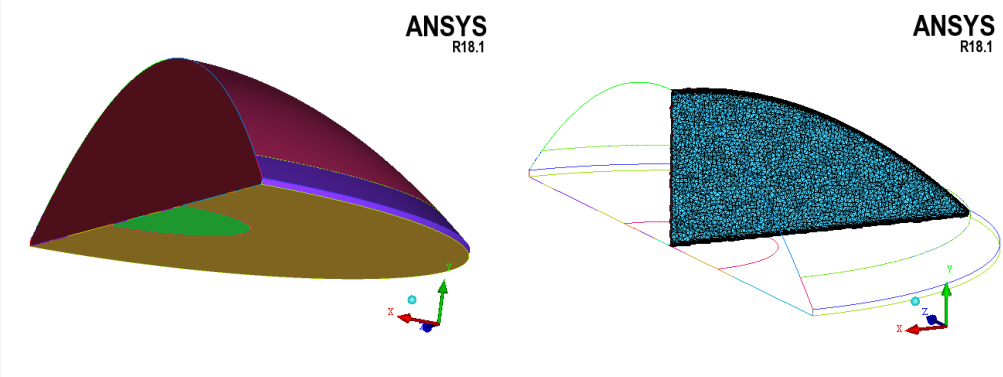

Figure 4. Geometry and a mesh slice.

A mesh convergence study was carried following the procedure established in Celik *et al.* (2008). The geometry, based on Eq. (1), is shown in Fig. 4. Four meshes were generated with ICEM CFD v18.1 software. They were named coarse, medium, fine and extra fine, with a constant grid refinement factor of $r = h_{coarser}/h_{finer} = 1.3$, where h is the characteristic cell length. The grids were hybrid, with triangular elements on the surface, tetrahedral in almost all the volume (Delaunay meshing algorithm) and prismatic at the walls, to better capture the gradients at this region. The average temperature was chosen as the representative convergence parameter, with results shown in Fig. 5. The fine mesh was considered suitable for the simulations, with a grid convergence index (GCI) of 0.2%.

For the simulation without flow through pupil, shown in Fig. 6, the boundary conditions were isothermal no-slip wall at the cornea, with $34,5°\mathrm{C}$, and at the iris/pupil, with $37°\mathrm{C}$, and symmetry on $y = 0$ plane.

With the numerical simulation, it is possible to observe the asymmetric effects caused by the gravitational acceleration,

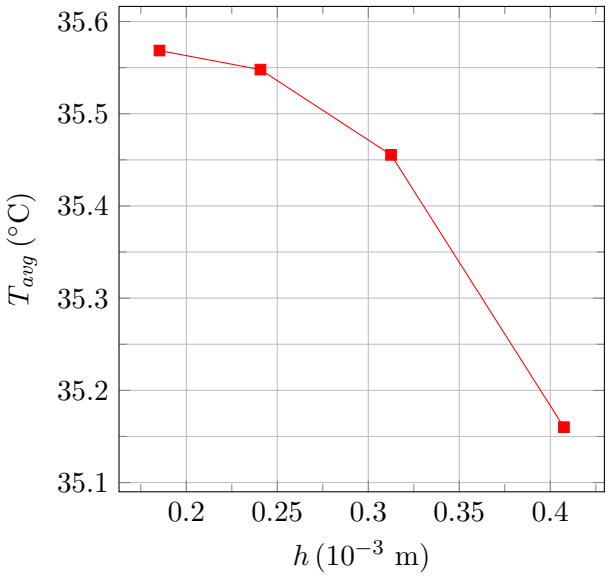

Figure 5. Average temperature as function of characteristic cell length h

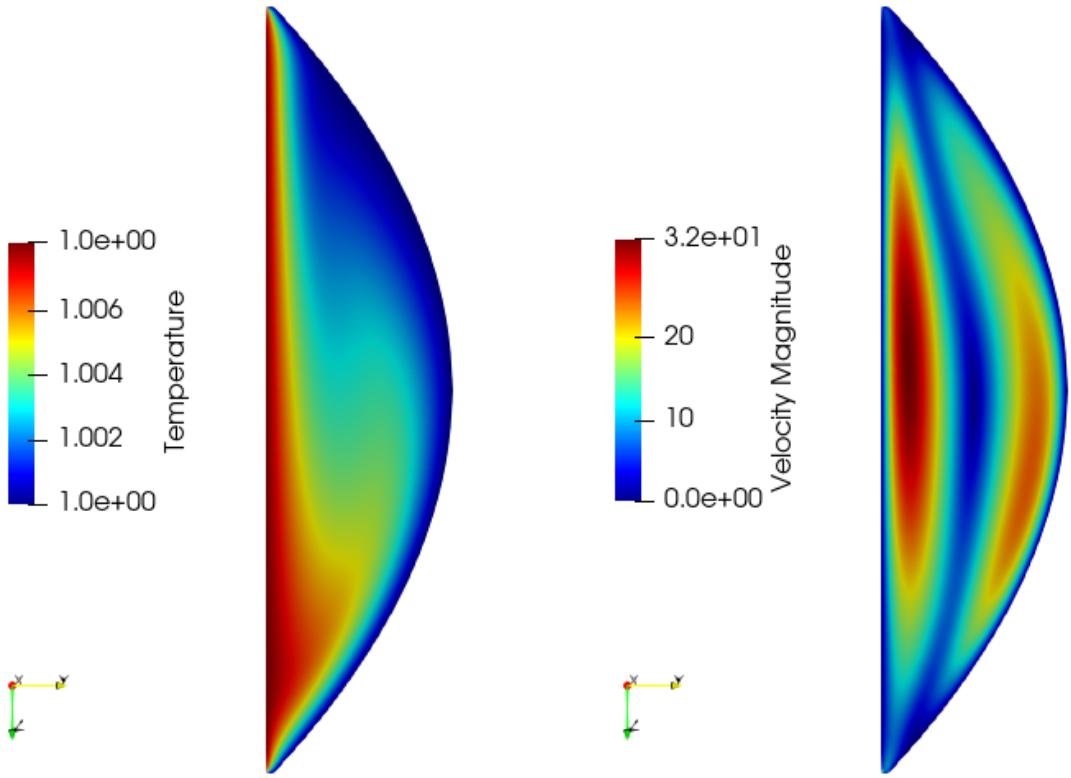

Figure 6. Contours of temperature (a) and velocity (b) at the central plane of the chamber, patient standing up without flow through pupil. Non-dimensional values.

both on temperature and velocity fields. In particular, the simplifications in the temperature equation previously discussed prevent capturing a region with higher temperatures at the bottom of the anterior chamber. As a consequence of this vertical temperature gradient, the two regions of maximum velocity are are slightly displaced, instead of being centralized as in the analytical solution.

For the isothermal case with flow through pupil, shown in Fig. 7, we imposed boundary conditions of velocity inlet and pressure outlet, in addition to no-slip at the walls. A flow of $3,0\ \mu\mathrm{L/min}$ was adopted, considering a patient lying down, i.e., gravitational acceleration does not contribute with asymmetries, and the flow is axissymetric. The resultants velocities magnitudes are more than one order of magnitude smaller than those of the isothermal flow with typical thermal gradients ($\sim 2°\mathrm{C}$).

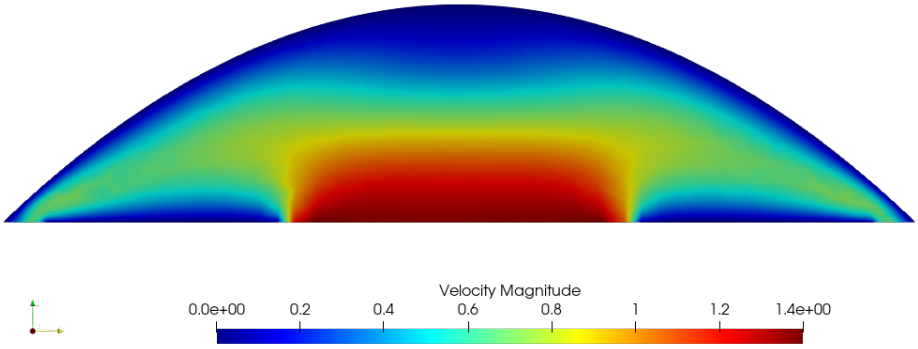

Figure 7. Contours of velocity, patient lying down without temperature gradient. Non-dimensional values.

4. CONCLUSIONS

It was shown, using analytical and numerical models, that the aqueous humour flow at the anterior chamber is buoyancy driven. Thus, even without flow through pupil, an internal flow occurs. For typical temperature gradients, for instance $2°$C, the associated velocities ($\sim 10^{-4}$ m/s) are more than one order of magnitude higher then the velocities associated with aqueous inflow/outflow. With the numerical solution, we were able to identify a temperature and velocity asymmetry of the flow to a patient standing up, what was not possible solely with analytical model.

5. REFERENCES

Batchelor, G.K., 1967. *An Introduction to Fluid Dynamics*. Cambridge University Press.

Brubaker, R.F., 1997. "Clinical measurements of aqueous dynamics: lmplications for addressing glaucoma". In *Current Topics in Membranes*, Elsevier, Vol. 45, pp. 233–284.

Canning, C.R., Greaney, M.J., Dewynne, J.N. and Fitt, A.D., 2002. "Fluid flow in the anterior chamber of a human eye". *Mathematical Medicine and Biology*, Vol. 19, No. 1, pp. 31–60.

Celik, I.B., Ghia, U., Roache, P.J. and Freitas, C.J., 2008. "Procedure for estimation and reporting of uncertainty due to discretization in cfd applications". *Journal of fluids Engineering-Transactions of the ASME*, Vol. 130, No. 7.

Fatt, I. and Weissman, B.A., 2013. *Physiology of the Eye: An Introduction to the Vegetative Functions*. Butterworth-Heinemann.

Goel, M., Picciani, R.G., Lee, R.K. and Bhattacharya, S.K., 2010. "Aqueous humor dynamics: a review". *The Open Ophthalmology Journal*, Vol. 4, p. 52.

Goldsmith, J.A., Li, Y., Chalita, M.R., Westphal, V., Patil, C.A., Rollins, A.M., Izatt, J.A. and Huang, D., 2005. "Anterior chamber width measurement by high-speed optical coherence tomography". *Ophthalmology*, Vol. 112, No. 2, pp. 238–244.

Karampatzakis, A. and Samaras, T., 2010. "Numerical model of heat transfer in the human eye with consideration of fluid dynamics of the aqueous humour". *Physics in Medicine & Biology*, Vol. 55, No. 19, p. 5653.

Kumar, S., Acharya, S., Beuerman, R. and Palkama, A., 2006. "Numerical solution of ocular fluid dynamics in a rabbit eye: parametric effects". *Annals of Biomedical Engineering*, Vol. 34, No. 3, p. 530.

Ng, E. and Ooi, E.H., 2007. "Ocular surface temperature: A 3D FEM prediction using bioheat equation". *Computers in Biology and Medicine*, Vol. 37, No. 6, pp. 829–835.

Pontes, J. and Mangiavacchi, N., 2016. *Fenômenos de Transferência com Aplicações às Ciências Físicas e à Engenharia Volume 1 (in Portuguese)*. Sociedade Brasileira de Matemática.

Poppendiek, H., Randall, R., Breeden, J., Chambers, J. and Murphy, J., 1967. "Thermal conductivity measurements and predictions for biological fluids and tissues". *Cryobiology*, Vol. 3, No. 4, pp. 318–327.

Tamm, E.R., 2015. "Functional morphology of the trabecular meshwork outflow pathways". In *Glaucoma*, Elsevier, pp. 40–46.

6. RESPONSIBILITY NOTICE

The authors are solely responsible for the printed material included in this paper.